Springer Ser Chem Sens Biosens (2007) 5: 111–149
DOI 10.1007/5346_025

Published online: 15 July 2006

Probing the Solid/Liquid Interface with the Quartz Crystal Microbalance

M. Urbakh (✉) · V. Tsionsky · E. Gileadi · L. Daikhin

School of Chemistry, Raymond and Beverly Sackler Faculty of Exact Sciences,
Tel-Aviv University, 69978 Ramat-Aviv, Israel
urbakh@post.tau.ac.il

Abstract In this chapter we discuss the results of theoretical and experimental studies of the structure and dynamics at solid–liquid interfaces employing the quartz crystal microbalance (QCM). Various models for the mechanical contact between the oscillating quartz crystal and the liquid are described, and theoretical predictions are compared with the experimental results. Special attention is paid to consideration of the influence of slippage and surface roughness on the QCM response at the solid–liquid interface. The main question, which we would like to answer in this chapter, is what information on

the structure and dynamics at the solid–liquid interface can be extracted from the QCM measurements. In particular, we demonstrate that the quartz crystal resonator acts as a true microbalance only if, in the course of the process being studied, the nature of the interface (its roughness, slippage, the density and viscosity of the solution adjacent to it, and the structure of the solvent in contact with it) is maintained constant.

So far most of the QCM data were analyzed on a qualitative level only. The next step in QCM studies requires a quantitative treatment of the experimental results. Theoretical basis for the solution of this problem already exists, and has been discussed in this review. Joint experimental and theoretical efforts to elevate the QCM technique to a new level present a challenge for future investigators.

Keywords Quartz crystal microbalance · Roughness · Slippage · Thin films

Abbreviations

a	Ratio of the slip length to the liquid decay length, b_s/δ
AFM	Atomic force microscope
C_m	Mass sensitivity of the QCM, $\frac{2f_0^2}{\sqrt{\mu_q \rho_q}}$
C_η	Sensitivity of the QCM operating in contact with a liquid, $\frac{f_0^{3/2}}{\sqrt{\pi \mu_q \rho_q}}$
d	Thickness of the quartz crystal
EQCM	Electrochemical quartz crystal microbalance
f	Frequency
f_0	Fundamental frequency of the resonator
$g(\boldsymbol{K})$	Correlation function for surface roughness
h	Root mean square height of a roughness
k	Wave vector of shear waves in quartz, $\omega\sqrt{\rho_q/\mu_q}$
l	Correlation length of surface roughness
d_f	Thickness of the liquid film
L	Thickness of interfacial layer
MD	Molecular dynamics
$P(\boldsymbol{r}, \omega)$	Pressure in a liquid
QCM	Quartz crystal microbalance
R	Hydrodynamic roughness factor
$\tilde{R}$	Electrochemical roughness factor
$\boldsymbol{r} = (z, \boldsymbol{R})$	Coordinates (normal and lateral)
SFA	Surface force apparatus
STM	Scanning tunneling microscope
$u(z, \omega)$	Amplitude of the shear displacements of the quartz
$u_f(\omega)$	Displacements of the homogeneous surface film
$v_f(t)$	Film velocity
$v_{f0}(\omega)$	Amplitude of film velocity
$v_q(t)$	Velocity of the quartz surface
$v_{q0}(\omega)$	Amplitude of the quartz surface velocity
$v_a(\omega)$	Velocity of absorbed later
$v_l(\omega)$	Liquid velocity at the interface
Z_L	Mechanical impedance of the contacting medium
Z_q	Mechanical impedance of quartz crystal
$\Delta\Gamma$	Half-width of the resonance

$\Delta\Gamma_l$	Half-width of the resonance for quartz crystal resonator contacting a semi-infinite liquid
Γ_a, Γ_m	Surface excess and maximum surface excess of adsorbate
δ	Velocity decay length in a liquid, $\delta = \sqrt{\eta/\pi\rho f_0}$
$\Delta\gamma$	Change of surface tension
Δf	Resonant frequency shift
Δf_m	Mass-induced resonant frequency shift
Δf_η	Viscosity-induced resonant frequency shift
Δf_P	Pressure-induced resonant frequency shift
Δf_R	Roughness-induced resonant frequency shift
Δf_{sl}	Slippage-induced resonant frequency shift
Δf_T	Resonant frequency shift due to change of temperature
Δf_l	Frequency shift for quartz resonator contacting a semi-infinite liquid
Δm_f	Surface mass density of a film
Δm_a	Average surface density of the adsorbed atoms
$\overline{\Delta m_f}$	Average surface mass density
Δm_1	Root mean square deviation of the mass distribution
$\varepsilon_{ls}, \varepsilon_{ll}$	Energy of liquid–substrate and liquid–liquid interactions
$\varepsilon_{la}, \varepsilon_{aa}, \varepsilon_{as}$	Energy of adsorbate–liquid, adsorbate–adsorbate and adsorbate–substrate interactions
η	Viscosity of a liquid
η_f	Viscosity of the liquid film
b_s	Slip length
b_s^{eff}	Effective slip length
λ_q	Wave length of shear-mode quartz oscillations
μ_q	Shear modulus of the quartz crystal
$\xi(\boldsymbol{R})$	Surface profile
ξ_H	Permeability of interfacial layer
ρ	Density of a liquid
ρ_q	Density of the quartz crystal
ρ_f	Density of the liquid film
ρ_s	Density of solid
τ_s	Slip time
ϕ	Porosity of interfacial layer
χ	Coefficient of sliding friction
ω	Angular frequency
ω_0	Fundamental angular frequency, $\omega_0 = 2\pi f_0$

1 Introduction

The literature concerning the quartz crystal microbalance (QCM) and its electrochemical analog, the electrochemical EQCM, is wide and diverse. Many reviews are available in the literature, discussing the fundamental properties of this device and its numerous applications, including its use in electrochemistry [1–7]. In this chapter we focus on the effect of interfacial properties on the QCM response, specifically when the device is immersed in a liquid.

When the quartz crystal microbalance was first introduced in 1959 [8], it represented a major step forward in our ability to weigh matter. Until then, routine measurements allowed a sensitivity of 0.1 mg, and highly sensitive measurements could be made with an accuracy limit of 0.03 μg, under well-controlled experimental conditions [9]. The QCM extended the sensitivity by two or three orders of magnitude, into the sub-nanogram regime.

Even when used in vacuum or in an inert gas at ambient pressure, the QCM acts as a balance only under certain conditions, as discussed below. Under these conditions the change of mass caused by adsorption or deposition of a substance from the gas phase can be related directly to the change of frequency, by the simple equation derived by Sauerbrey [8].

Generally this is not the case, and the frequency shift observed could more appropriately be expressed by a sum of terms of the form:

$$\Delta f = \Delta f_{\mathrm{m}} + \Delta f_{\eta} + \Delta f_{\mathrm{P}} + \Delta f_{\mathrm{R}} + \Delta f_{\mathrm{sl}} + \Delta f_{\mathrm{T}} \,, \tag{1}$$

where the different terms on the right hand side of this equation represent the effects of mass loading; viscosity and density of the medium in contact with the vibrating crystal; the hydrostatic pressure; the surface roughness; the slippage effect, and the temperature, respectively, and the different contributions can be interdependent. These effects become of major importance particularly when small changes of frequency, associated with sub-monolayer phenomena, are considered. Some of these factors will be discussed in this chapter.

1.1 Applications of the Quartz Crystal Microbalance

The most common commercial use of the QCM is as a thickness gauge in thin-layer technology. When used to monitor the thickness of a metal film during physical or chemical vapor deposition, it acts very closely as a nanobalance, providing a real-time measurement of the thickness. Indeed, devices sold for this purpose are usually calibrated in units of thickness (having a different scale for each metal, of course), and claim a sensitivity of less than 0.1 nm, which implies a sensitivity of less than a monolayer.

The other common application of the QCM is as a nanosensor proper, made sensitive to one gas or another by suitable surface treatment. Selecting the suitable coating on the electrodes of the QCM can determine selectivity and enhance sensitivity. It is not our purpose to discuss sensors in the present review. It should only be pointed out that any such sensor would have to be calibrated, since the Sauerbrey equation would not be expected to apply quantitatively.

1.2 Applications for Gas-Phase Adsorption

The high sensitivity of the QCM should make it an ideal tool for the study of adsorption from the gas phase. We note that the number of sites on the surface of a metal is typically of the order of 10^{15} cm^{-2}, hence a monolayer of a small adsorbate, occupying a single site, would be about 2 nmol cm^{-2}. A monolayer of water would therefore weigh about 40 ng cm^{-2}, while a monolayer of pyridine would weigh 30–60 ng cm^{-2}, depending on its orientation on the surface. Comparing these numbers with the sensitivity of 2 ng cm^{-2} shows that adsorption isotherms could be measured in the gas phase, employing the QCM. This has not been done properly until relatively recently, mainly because the device was treated as a microbalance, i.e., it was assumed that the Sauerbrey equation could be applied, and several important terms in Eq. 1 were ignored. Obtaining adsorption isotherm one has to change the pressure over a wide range. Therefore the changes of properties of the surrounding gas cannot be ignored. This shortcoming was overcome by the present authors [10] who developed the *supporting gas method*. When this method is employed, the overall pressure is maintained constant by a large excess of an inert gas, and the frequency shift of the QCM is measured as a function of the partial pressure of the material being investigated. In this manner all terms in Eq. 1, other than Δf_m, are essentially zero and the device acts as a true nanobalance.

1.3 Use of the QCM in Liquids

It was not initially obvious that the quartz crystal resonator would operate in liquids, until this was proven experimentally [11, 12]. The term associated with the influence of the viscosity, η, and density, ρ, of liquid in Eq. 1 can be written [13] as:

$$\Delta f_\eta = - C_\eta \left(\eta\rho\right)^{1/2} \ . \tag{2}$$

Since the product of $\sqrt{\eta\rho}$ in liquids is about two orders of magnitude higher than in gases at ambient pressure, the crystal is heavily loaded when transferred from the gas phase into a liquid.

Once the door had been opened to its use in liquids, the potential of the QCM for interfacial electrochemistry was obvious, and the EQCM became popular.

When a QCM, with fundamental frequencies 6–10 MHz, is placed in contact with a dilute aqueous solution, the frequency should shift to lower values by about 0.8–1.2 kHz according to Eq. 2. In practice the observed shift is larger by 1–2 kHz, depending on the surface roughness. The effect of roughness is also related indirectly to viscosity and density, since the hydrodynamic

flow regime at the surface is altered as a result of roughness [14–16]. Roughness is a major issue in the interpretation of the response of the QCM in liquids, and it is discussed in some detail in the following sections.

1.4 Impedance Spectrum of the EQCM

In early studies of the QCM and the EQCM, only the resonance frequency was determined, and conclusions were drawn, based on the shift of frequency. Unfortunately, in many cases this shift was attributed to mass loading alone, and it was used to calculate the weight added or removed from the surface, disregarding other factors that affect the frequency. In the past decade more and more laboratories expanded such studies to include measurements of the impedance spectrum of the crystal [17–28]. This provides an additional experimental variable that can obviously yield further information and deeper understanding of the structure of the interface. For instance, a variation of the resonance width provides an unambiguous proof that mechanisms other than mass loading are also involved.

The properties of the impedance spectrum are discussed in detail in Chap. 2 in this volume. Here we present only a relation between the resonant frequency and the mechanical impedance of the medium contacting the quartz surface, Z_L. The latter is defined as the ratio of the shear stress acting on the contact medium to the surface velocity [6]. Under the experimental conditions when the surface loading is relatively small, the shift of the resonant frequency with respect to the resonant frequency of the unloaded quartz crystal, f_0, can be written as [14, 29]:

$$\Delta\tilde{f} \equiv \Delta f + i\Delta\Gamma = i\frac{f_0}{\pi}\frac{Z_L}{Z_q}, \tag{3}$$

where Z_q is the acoustic impedance of an AT-cut quartz.

It should be noted that the frequency shift $\Delta\tilde{f}$ can be a complex number, and its imaginary part, $\Delta\Gamma$, reflects the half-width of the resonance. Equation 3 shows that the complex frequency shift $\Delta\tilde{f}$ contains the same information as the mechanical impedance Z_L.

In order to analyze the influence of the different loading mechanisms on the QCM response one has to model a dependence of the mechanical impedance Z_L or the complex resonance frequency shift on the chemical and physical properties of the contacting medium. Various models for the mechanical contact between the oscillating quartz crystal and the outer medium are discussed below. The QCM is now so widely and extensively used that, in the framework of this chapter, it is not possible to review all the available literature. Hence we limited ourselves here to a review of the experimental data and theoretical ideas concerning the studies of structure and interaction at solid–liquid interface. Furthermore, we did not present here studies on

adsorption, metal deposition, and kinetics with the help of the QCM. These topics are well described in previous reviews ([1, 2, 6], and in many articles published in readily accessible journals). The problems of the interpretation of the QCM response caused by changes taking place at the solid–liquid interface are obviously of first priority, especially for studies in electrochemistry.

2
Effect of Thin Surface Films

2.1
Film Rigidly Attached to the Surface

First we consider the effect of a thin film, rigidly attached to an ideally flat crystal surface, on the response of the quartz crystal resonator (Fig. 1).

For a homogeneous thin film with a thickness smaller than the wavelength of the shear oscillations, the shift of the resonance frequency can be expressed in terms of the change in surface mass density of the film, Δm_f, (in units g cm^{-2}). This was given by Sauerbrey [8] as:

$$\Delta f = - C_m \Delta m_f \,, \tag{4}$$

where $C_m = 2f_0^2/(\mu_q \rho_q)^{1/2}$ and ρ_q and μ_q are the density and shear modulus of quartz. Equation 4 can be derived by supplementing the wave equation, which describes displacements in the quartz crystal, with the Newtonian equation of motion for the surface film [6]. Equation 4 shows that the addition of mass rigidly attached to the surface of the quartz crystal resonator leads to a decrease of the resonant frequency, but it does not influence the width of

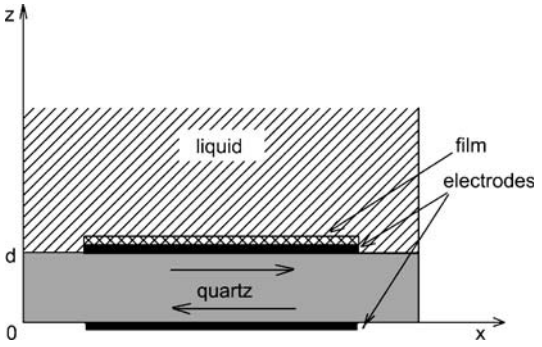

Fig. 1 Schematic presentation of the quartz crystal resonator in contact with a liquid. The contacting medium is a thin film rigidly attached to the crystal surface from one side, at $z = d$. The opposite surface of the crystal ($z = 0$) is unconstrained. d is the thickness of the quartz crystal

the resonance. The constant C_m in Eq. 4 can differ from the theoretical value given above due to effects of non-uniform mass distribution, roughness, etc. Therefore one is well advised to calibrate the QCM.

It should be noted that Eq. 4 is valid only for thin films for which the thickness is much smaller than the wave length of the shear mode oscillations. In this case the frequency shift is determined by the inertial force of the film acting on the quartz surface. For thicker films effects of elasticity or viscoelasticity become important and Eq. 4 should be modified essentially [30].

A question arises whether an inhomogeneous mass distribution would lead to an additional shift of frequency and/or to a broadening of the resonance, compared to the result given by the Sauerbrey equation? It was shown [6] that in the case of inhomogeneous mass distribution splitting of the resonant frequency can occur, and the frequency shift can be estimated as:

$$\Delta f = - \frac{2f_0^2}{\sqrt{\rho_q \mu_q}} [\overline{\Delta m}_f \pm \Delta m_1] , \tag{5}$$

where Δm_1 is the root mean square deviation of the mass density from the average value $\overline{\Delta m}_f$. In contrast to the case of uniform mass loading, where $\Delta m_1 = 0$, two values of the resonance frequency are derived. This effect can be simulated by a simple equivalent circuit consisting of two Butterworth–Van Dyke [31–33] circuits in series with the inductances corresponding to the two different values of the surface mass densities, $\overline{\Delta m}_f + \Delta m_1$ and $\overline{\Delta m}_f - \Delta m_1$. Due to overlap of these two resonance states, splitting can lead to an apparent broadening of the resonance, which will have an effective half-width of the order of $f_0^2 \Delta m_1 / \pi (\mu_q \rho_q)^{1/2}$. For the 6 MHz quartz resonator this broadening effect becomes important when the correlation length of the mass distribution is larger than 0.02 cm.

2.2 Slippage at the Interface Between a Thin Film and a Solid

The Sauerbrey equation shows that a thin uniform film rigidly attached to the quartz surface does not influence the width of the mechanical resonance. However, it was experimentally shown for a number of systems that adsorption on the quartz surface produced both a shifts of frequency and an increase of the width of the resonance [34–38]. This phenomenon can be explained, assuming slippage at the adsorbate–substrate interface.

Slippage occurs as a result of the force of inertia acting on the adsorbate during the vibrational motion of the crystal. The force of inertia, $\boldsymbol{F}$, is extremely weak ($\sim 10^{-13}$ dyne per atom) [39] and cannot, by itself, move an adsorbed species over the lateral energy barriers of the adsorbate–substrate potential [39]. However, this force decreases the barriers in the direction of $\boldsymbol{F}$ that leads to a thermally activated drift of the adsorbate in the direction oppo-

site to the motion of the crystal surface. As a result, the instantaneous velocity in the adsorbate layer can differ from the velocity of the surface of the quartz crystal resonator.

The slippage at the interface between a thin film of density Δm_f and the substrate is usually described in terms of an interfacial friction coefficient ("coefficient of sliding friction"), χ. This coefficient determines the stress acting between the film and the substrate, which move at different velocities. An infinite value of χ implies that the non-slip (sticking) boundary condition is applicable. When the interfacial friction coefficient equals zero, the film is free to slide with no energy dissipation.

The motion of the adsorbed film on the oscillating quartz surface can be described by Eq. 6:

$$\Delta m_f \frac{d}{dt} v_f(t) = -\chi [v_f(t) - v_q(t)] , \tag{6}$$

where $v_q(t) = v_{q0}(\omega) \exp(i\omega t))$ and $v_f(t) = v_{f0}(\omega) \exp(i\omega t)$ are the velocities of the crystal surface and of the film. Simultaneous solution of the wave equation in the quartz crystal and the equation of motion (Eq. 6) for the adsorbed film yields the following expressions for the changes of the frequency, Δf, and the half-width of the resonance,$\Delta \Gamma$:

$$\Delta f = -\frac{2f_0^2 \Delta m_f}{\sqrt{\rho_q \mu_q}} \left[\frac{\chi^2}{\chi^2 + (2\pi f_0 \Delta m_f)^2} \right] \tag{7}$$

$$\Delta \Gamma = \frac{2f_0^2 \Delta m_f}{\sqrt{\rho_q \mu_q}} \left[\frac{2\pi f_0 \Delta m_f \chi}{\chi^2 + (2\pi f_0 \Delta m_f)^2} \right] . \tag{8}$$

Note that:

$$\frac{\Delta \Gamma}{\Delta f} = -2\pi f_0 \frac{\Delta m_f}{\chi} . \tag{9}$$

Thus, the interfacial friction can be evaluated from measurement of $\Delta \Gamma$ and Δf. This procedure has been applied to a number of systems in which weak physical adsorption occurs, such as the adsorption of Xe, Kr, N_2 on Au, and of H_2O and C_6H_{12} on Ag [34–38]. In all the above cases slippage was observed, and the ratio of the coefficient of sliding friction to the mass density was of the order $\chi/\Delta m_f = (10^8 - 10^9)\,s^{-1}$. As an example, the frictional stress acting on the monolayer Xe film sliding on a Ag(111) surface at a velocity $v = 1\,cm\,s^{-1}$, $F = \chi v$, equals about $10\,Nm^{-2}$ [40]. It is much smaller than typical shear stresses involved in sliding of a steel block on a steel surface under boundary lubrication condition (Eq. 6), which is of order $\approx 10^8\,Nm^{-2}$ [39].

The effect of slippage at a substrate–film interface can also be described in terms of slip time [39]. To understand the physical meaning of the slip time, one can consider an adsorbate film on a substrate, moving at constant velocity. If the substrate stops, the velocity and momentum of the film decay exponentially, and the time constant of this process is the slip time. If this process is very rapid, i.e., we have a rigidly adsorbed film, the time constant will be close to zero, and there will be no noticeable slip. The slip time is related to the interfacial friction coefficient through the equation [39]:

$$\tau_s = \Delta m_f / \chi \, . \tag{10}$$

In a recent paper [41] the dependence of the slip time, τ_s, on the amplitude of the crystal surface oscillations, A, and on the surface coverage was investigated. The results refer to the absorption of krypton atoms on gold at 85 °K. It was found that there is a step-like transition between a low-coverage region, where slippage exists at the solid–film interface, and a high-coverage region where the film is locked to the surface. The transition occurs at different coverage depending on the amplitude, A. Independent of coverage, the film is attached rigidly to the surface for $A \leq 0.18$ nm and slides for $A > 0.4$ nm. In the region of sliding at small coverages the values of the slip time are in the interval 2–10 ns, for $0.18 \text{ nm} < A < 0.4$ nm.

3
Quartz Crystal Operating in Contact with a Liquid

3.1
General Considerations

When a quartz crystal resonator operates in contact with a liquid, the shear motion of the surface generates motion in the liquid near the interface. The velocity field, $\boldsymbol{v}(\boldsymbol{r}, \omega)$, related to this motion in a semi-infinite Newtonian liquid is described by the linearized Navier–Stokes equation:

$$i\omega\rho\boldsymbol{v}(\boldsymbol{r}, \omega) = -\nabla P(\boldsymbol{r}, \omega) + \eta\Delta\boldsymbol{v}(\boldsymbol{r}, \omega) \, , \tag{11}$$

where $P(\boldsymbol{r}, \omega)$, η and ρ are pressure, viscosity, and density of the liquid. Under the typical conditions of the QCM experiments, where the shear velocities are much smaller than the sound velocity in the liquid, the displacement of the crystal does not generate compressional waves and a liquid can be considered to be incompressible. If the surface is sufficiently smooth, the quartz oscillations generate plane-parallel laminar flow in the liquid, as shown in Fig. 2. The velocity field obtained as the solution of Eq. 11 for a flat surface has the form:

$$v_x(z) = v_{q0}(\omega) \exp[-(1 + i)z/\delta] \, , \tag{12}$$

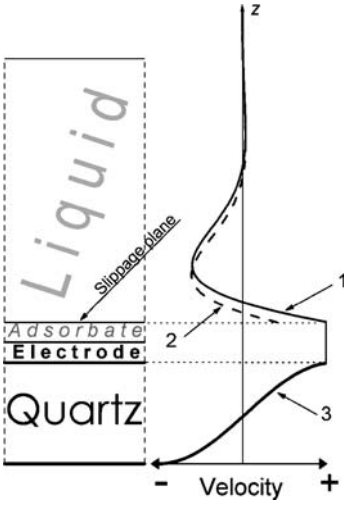

Fig. 2 System geometry and velocity profiles. *Curves 1* and *2* represent the velocity distributions at the liquid–adsorbate interface without and with slippage, respectively. *Curve 3* is the velocity distribution in the quartz. The thickness of various layers is not drawn to scale

where $v_{q0}(\omega)$ is the velocity of the liquid at the surface, and $\delta = \sqrt{2\eta/\omega_0\rho}$. Equation 12 represents a damped shear wave radiating into the liquid from the surface of the oscillating resonator. δ is the velocity decay length of this shear wave, which lies between 250 and 177 nm for dilute aqueous solutions at room temperature, for crystals having a fundamental frequency in the range 5–10 MHz. Damping of the shear wave has a number of important consequences. First, it ensures that the quartz crystal can operate in liquids, the losses in the liquid being limited by the finite depth of penetration. Secondly, a small portion of the liquid is coupled to the crystal motion and a frequency decrease is observed. Thirdly, the viscous nature of motion gives rise to energy losses, which are sensed by the resonator, both as a decrease in frequency and as an increase in the width of the resonance.

3.2
Non-slip Boundary Condition

The response of the QCM at the solid–liquid interface can be found by matching the stress and the velocity fields in the medium in contact. It is usually assumed that the relative velocity at the boundary between the liquid and the solid is zero. This corresponds to the non-slip boundary condition. Strong experimental evidence supports this assumption on the macroscopic scales [42, 43]. In this case the frequency shift, Δf_l, and the half-width of the

resonance, $\Delta\Gamma_l$, can be written as follows [12, 13]:

$$\Delta f_l = -\frac{f_0^{3/2}\sqrt{\rho\eta}}{\sqrt{\pi\rho_q\mu_q}} \tag{13}$$

$$\Delta\Gamma_l = \frac{f_0^{3/2}\sqrt{\rho\eta}}{\sqrt{\pi\rho_q\mu_q}}\,. \tag{14}$$

Equations 13 and 14 show that the generation of a damped laminar flow in the liquid causes a decrease in the resonance frequency and an increase in the resonance width, which are both proportional to $\sqrt{\rho\eta}$. In contrast to the case of the mass loading where Δf is proportional to f_0^2, the liquid-induced response of the QCM is proportional to $f_0^{3/2}$.

It is interesting to note that for both a surface film rigidly attached to the resonator and a liquid in contact with the surface of the quartz crystal, the shift of the resonant frequency can be written in the same form, as:

$$\Delta f = -f_0\frac{\rho}{\rho_q}kh_{\text{eff}}\,. \tag{15}$$

Where $k = \omega_0\sqrt{\rho_q/\mu_q}$, ρ is the bulk density of the medium in contact with the vibrating surface of the solid, a film or a liquid, and h_{eff} is the thickness of the layer that responds to the quartz oscillations. In the case of the film, h_{eff} coincides with the thickness. For a semi-infinite liquid, h_{eff} presents a thickness of liquid involved in the motion and it should be taken as equal to $\delta/2$. The difference in the frequency dependence of the QCM response in the two cases is a result of the frequency dependency of δ. However, in contrast to the case of pure mass loading, the effect of a liquid results not only in a frequency shift but also in a broadening of the resonance.

3.3 Effect of a Thin Liquid Film at the Interface

The properties (the effective viscosity and density) of the liquid layer in close vicinity to the interface can differ from their bulk values. There are various reasons for these phenomena. For example, the structuring of a liquid induced by the substrate and a non-uniform distribution of species in the liquid near the substrate can influence significantly the properties of the liquid at the interface. The liquid properties change with distance from the interface, until the values corresponding to the bulk of solution have been reached. In order to simplify the description of this non-uniformity on the QCM, we assume here that a thin film of liquid, having different values of η_f and ρ_f, exists at the interface [44]. To calculate the effect of this film on the frequency shift,

one has to solve the wave equation for the elastic displacements in the quartz crystal simultaneously with the linearized Navier–Stokes equation for the velocities in the film and in the bulk liquid under standard non-slip boundary conditions.

Then the shift of the resonant frequency and the half-width of the resonance can be written as:

$$\Delta f = -\frac{f_0^{3/2}\sqrt{\rho\eta}}{\sqrt{\pi\mu_q\rho_q}} - \frac{2f_0^2}{\sqrt{\mu_q\rho_q}}\left[\rho(1-\frac{\eta}{\eta_f}) + (\rho_f - \rho)\right] d_f \tag{16}$$

$$\Delta\Gamma = \frac{f_0^{3/2}\sqrt{\rho\eta}}{\sqrt{\pi\mu_q\rho_q}} + \frac{2f_0^2}{\sqrt{\mu_q\rho_q}}\left[\rho(1-\frac{\eta}{\eta_f}) + (\rho_f - \rho)\right] \frac{d_f^2}{\delta}\,. \tag{17}$$

Here d_f and ρ_f are the thickness and the density of the film. These equations are valid in a particular case, when $d_f \ll \delta$. The general case for arbitrary d_f was given in [44]. The first terms in Eqs. 16 and 17 yield the liquid-induced frequency shift and half-width of the resonance in the absence of a film. The terms in brackets describe the influence of the viscosity and density of a film of thickness d_f. According to Eqs. 16 and 17, the ratio of the film-induced half-width to the film-induced frequency shift is proportional to d_f/δ. Thus, for $d_f/\delta \ll 1$, the contribution of the thin interfacial film to the width is much smaller than its contribution to the frequency shift. For $\eta_f \gg \eta$ the film acts as though it were rigidly attached to the surface: it causes a shift in frequency equal to that caused by its mass. The thin film model has been successfully used to describe the QCM response in electrochemical systems, which arises due to the effect of electrostatic adsorption of ions and the effect of electric field on viscosity inside the diffuse layer [44].

3.4
Slip Boundary Conditions

3.5
Slippage at Solid–Liquid Interface

Although the non-slip boundary condition has been remarkably successful in reproducing the characteristics of liquid flow on the macroscopic scale, its application for a description of liquid dynamics in microscopic liquid layers is questionable. A number of experimental [45–52] and theoretical [53, 54] studies suggest the possibility of slippage at solid–liquid interfaces. Recent reviews [55–57] summarize the results of these works. Here we focus on the effect of slippage on the QCM response.

The boundary condition is controlled by the extent to which the liquid "feels" a spatial corrugation in the surface energy of the solid. This depends

on a number of interfacial parameters, including the strength of the liquid–liquid and liquid–solid interactions, the commensurability of the substrate and the liquid structures, substrate and liquid densities, and also the roughness of the interface. In order to quantify the slippage effect, the slip length, b_s, is usually introduced [53, 58, 59]. The traditional non-slip boundary condition is replaced by:

$$\left.\frac{dv(z,\omega)}{dz}\right|_{z=0} = \frac{1}{b_s}(v(0,\omega) - v_{q0}(\omega)) , \tag{18}$$

where $v(z,\omega)$is the velocity in the liquid and $v_{q0}(\omega)$ is the velocity of the quartz crystal surface, $z = 0$. Equation 18 expresses the discontinuity of the velocity across the interface. For $b_s = 0$, Eq. 18 is reduced to the usual non-slip boundary condition: $v(d,\omega) = v_{q0}(\omega)$. The physical meaning of the slip length can be clarified by comparing velocity profiles for the non-slip and slip boundary conditions. These two profiles coincide when the non-slip boundary condition is imposed at the surface shifted inside the solid by the distance b_s with respect to the actual interface.

Basically two different types of experimental approaches have been used to study the boundary slip: local (direct) [45, 60] and effective (indirect) methods [49–52, 61]. The first group of methods is based on application of optical techniques using tracer particles or molecules to determine the flow field. These techniques have a resolution of less than 100 nm, so they cannot distinguish small differences in slip lengths. The effective methods assume the boundary conditions (Eq. 18) or similar ones to hold at the substrate surface and infer the slip length by measuring macroscopic quantities. These methods have been the most popular so far and they include atomic force microscopy (AFM), surface force apparatus (SFA), capillary techniques, and QCM.

The experimental studies involving different techniques report slip effects varying over more than two orders of magnitude, and with qualitatively different shear-rate dependence, for similar systems [55, 56]. Drastically different behaviors are reported for liquids wetting atomically smooth surfaces [45, 49, 55, 56, 62], for the influence of surface roughness [63, 64], and for the amplitude and rate dependence of boundary slip on hydrophobic surfaces [48–52]. There is no clear understanding why such large differences are obtained. A possible reason for the disagreement between the results obtained by different groups is a contamination of substrate surfaces by nanoparticles [49, 65]. Another parameter of obvious importance, which may explain such variability, is surface roughness. We discuss the effect of roughness on slippage in Sect. 5 of this chapter.

Within the QCM measurements the slip boundary condition (Eq. 18) results in the following equations for the resonant frequency shift and the

half-width of the resonance:

$$\Delta f = -\frac{f_0^2 \rho \delta}{\sqrt{\rho_q \mu_q}} \left[\frac{1}{(1 + b_s/\delta)^2 + (b_s/\delta)^2} \right] \approx -\frac{f_0^2 \rho \delta}{\sqrt{\rho_q \mu_q}} \left[1 - \frac{2 b_s}{\delta} \right] \tag{19}$$

$$\Delta \Gamma = \frac{f_0^2 \rho \delta}{\sqrt{\rho_q \mu_q}} \left[\frac{1 + 2\lambda/\delta}{(1 + b_s/\delta)^2 + (b_s/\delta)^2} \right] \approx \frac{f_0^2 \rho \delta}{\sqrt{\rho_q \mu_q}} \left[1 - \frac{2 b_s^2}{\delta^2} \right], \tag{20}$$

where the right hand side equalities are valid for small values of the slip length, $b_s/\delta \ll 1$. Equations 19 and 20 show that the influence of the slippage on the response of the QCM in liquid is determined by the ratio of the slip length b_s to the velocity decay length, δ. Even for a small value of $b_s \approx 1$ nm the slippage-induced correction to the frequency shift, Δf_{sl}, will be of the order of 6.5 Hz for the fundamental frequency of $f_0 = 5$ MHz. This value far exceeds the resolution of the QCM, but it is difficult to separate it from the overall QCM signal.

It should be noted that in QCM measurement interfacial properties are determined by averaging over the length scale δ. As a result one cannot distinguish between a true slip on the molecular level and an apparent hydrodynamic slip, which can arise from a shear thinning of the liquid near the surface. The latter leads to a steep velocity profile at the surface that appears as a slip, although the velocity is continuous at the surface. Indeed, a comparison between Eqs. 19–20 and Eqs. 16–17, which describe the effects of slip and surface film on the resonant frequency respectively, allow a relationship to be established between the apparent slip length and the film properties that give the same QCM response:

$$\frac{b_s}{\delta} = \left(\frac{\eta}{\eta_f} - \frac{\rho_f}{\rho} \right). \tag{21}$$

According to Eq. 21 the apparent boundary slip can be observed if the viscosity and/or density depends on the composition ($\eta \neq \eta_f$, $\rho \neq \rho_f$) and the less viscous and less dense fraction of the liquid wets the substrate better than the more viscous and the more dense one ($\eta > \eta_f$, $\rho > \rho_f$). It is also clear that there are two ways to obtain a large slip length. The first is by having a macroscopically thick boundary layer, since the slip length has the same order of magnitude as the thickness of this layer. The second is by providing large values of the viscosity and/or density contrast. Similar conclusions were reached in [66] for the Couette flow of liquid.

There were attempts [39] to estimate the slip length at the solid–liquid interface on the basis of QCM experiments for adsorbed liquid layers. The slip length can be expressed in terms of the coefficient of sliding friction, χ, at the

interface:

$$b_s = \frac{\eta}{\chi} . \tag{22}$$

Using the sliding friction coefficient $\chi = 3\,\mathrm{g\,cm^{-2}\,s^{-}}$, which is obtained for a monolayer of water on Ag in [35] and on Au in [67], a surprisingly high slip length of $b_s = 6 \times 10^4$ nm is obtained. Using this value for the interface between Au and bulk water, Eq. 19 yields for $f_0 = 5$ MHz a value of $\Delta f \approx 7 \times 10^{-3}$ Hz, which turns out to be smaller than that observed experimentally by a factor of 10^5. This inconsistency is most likely caused by a roughness of the electrode surface that reduces the effective slip length. Another reason could be the difference between friction at the solid–adsorbed layer and the solid–liquid interfaces. For example, a decrease of the slip length with increasing film thickness has been observed recently in QCM studies of Kr films on gold electrodes [41].

From a theoretical point of view, molecular dynamics simulations (MD) have shown [53, 66, 68] that the slip length is mostly determined by the ratio of characteristic energies of liquid–substrate, ε_{ls} and liquid–liquid ε_{ll} interactions, $b_s = f(\varepsilon_{ls}/\varepsilon_{ll})$. For the simple Lennard–Jones liquids wetting an atomically smooth surface, $\varepsilon_{ls}/\varepsilon_{ll} \geq 1$, slip length is negligible except at very high shear rate when the hydrodynamic boundary condition becomes nonlinear [53, 68]. It grows with the decrease of the parameter $\varepsilon_{ls}/\varepsilon_{ll}$. Substantial slip develops in non-wetting situations when the contact angle is larger than 90°, with slip lengths reaching 10–50 molecular sizes, and it depends on the pressure [59]. It should also be noted that, for a given value of $\varepsilon_{ls}/\varepsilon_{ll}$, the slip length is minimal when substrate and liquid molecules are of the same size, and increases with the increase of incommensurability of the sizes. For smaller coupling between the liquid and the substrate or incommensurability of their sizes, the spatial corrugation in the interfacial energy is weaker and interfacial slip can develop.

MD simulations and mode-coupling calculations [59, 68, 69] have shown that the magnitude of the hydrodynamic slippage can be correlated to the wettability of surfaces, which is characterized by a contact angle θ [59]:

$$\cos(\theta) = -1 + 2\frac{\rho_s}{\rho}\frac{\varepsilon_{ls}}{\varepsilon_{ll}} , \tag{23}$$

where ρ_s and ρ are the density of the solid and the liquid, respectively. Thus, the contact angle may be interpreted as a measure of the strength of interaction between the liquid and the solid, ε_{ls}. One expects a large value of the slip length for a non-wetting situation ($\cos(\theta) \to -1$), when ε_{ls} becomes much smaller than ε_{ll}. This conclusion is in agreement with several experimental observations [45, 70] reporting large slip lengths for partially wetting liquids.

An early model for molecular slip based on wetting properties has been suggested by Tolstoi [71] and extended in later publications [72]. This model

predicts a relation between the slip length and the contact angle in the form

$$b_s/\sigma = \exp\left[\alpha\sigma^2\gamma\left(1-\cos\theta\right)/k_BT\right]-1\,, \tag{24}$$

where σ is the molecular size, γ is the surface tension at the substrate–liquid interface and α is a geometric parameter of order one. According to Eq. 24 the slip length increases with the contact angle and can be orders of magnitude above the molecular length. However, the values predicted by Eq. 24 are usually much smaller than those measured experimentally. As well, Eq. 24 does not account for surface roughness or other surface properties.

The authors of [16, 73, 74] showed that surface treatments affecting liquid contact angle influence the response of quartz crystal resonator: resonant frequency changes caused by liquid loading were consistently smaller for surfaces having large liquid contact angles. These results were interpreted as arising from the onset of slippage at the solid–liquid interface: the solid–liquid interaction becomes sufficiently weak on a hydrophobic surface and shear displacement becomes discontinuous at the interface. However, this interpretation was called into question by a series of experiments, in which the effect of a hydrophobic monolayer was examined on devices with various surface roughness [14].

3.6
Slippage at the Adsorbate–Electrolyte Interface

Slippage is very sensitive to the molecular structure of the interface, as we have already discussed. Thus, adsorption can strongly influence this phenomenon. In order to describe the effect of adsorption, let it be assumed that the adsorbed layer is rigidly attached to the surface, and slippage occurs at the adsorbate–liquid interface, see Fig. 2. Then the equation of motion of the adsorbed layer can be written as [61]:

$$i\omega\Delta m_a v_a(\omega) = -\mu_q\frac{du(z)}{dz} - \chi(v_a(\omega)-v_l(\omega))\,,\quad \text{at}\quad z=d\,, \tag{25}$$

where $v_a(\omega)$ is the velocity of the adsorbed layer and Δm_a is its mass per unit area, while $v_l(\omega)$ is the velocity of the liquid at the interface, $z = d$. The first term on the right hand side of Eq. 25 describes the driving force acting on the adsorbed layer from the quartz crystal, while the second term accounts for the friction at the adsorbate–liquid interface.

The velocity fields in the crystal and the liquid are given by the solutions of the wave equation in the crystal and the linearized Navier–Stokes equation in the liquid, respectively. The solution of these equations and Eq. 25, with the boundary conditions for shear stresses and velocities, leads to the following equation for the shift of the resonant frequency, Δf, and the change of the

half-width of the resonance, $\Delta\Gamma$:

$$\Delta f = -\frac{2f_0^2\Delta m_a}{(\rho_q\mu_q)^{1/2}} - \frac{f_0^{3/2}(\rho\eta)^{1/2}}{(\pi\rho_q\mu_q)^{1/2}}\left[\frac{1}{(1+a)^2+a^2}\right] \tag{26}$$

$$\Delta\Gamma = \frac{f_0^{3/2}(\rho\eta)^{1/2}}{(\pi\rho_q\mu_q)^{1/2}}\left[\frac{(1+2a)}{(1+a)^2+a^2}\right]. \tag{27}$$

Writing Eqs. 26 and 27 we introduced a dimensionless parameter $a = \eta/\chi\delta = b_s/\delta$, which is the ratio of the slip length, $b_s = \eta/\chi$, and the velocity decay length in the liquid, δ. Equations 26 and 27 include both the interfacial (adsorption) and the bulk solution contributions to the response of the QCM, given by Eqs. 13 and 14. The latter remains constant in adsorption studies, and can be subtracted from the overall change given by Eqs. 26 and 27. As a result, the shift of the resonant frequency and the change of the half-width due to adsorption, which are measured experimentally, are given by the equations:

$$\Delta f - \Delta f_l \equiv \Delta f_m + \Delta f_{sl} = -\frac{2f_0^2\Delta m_a}{(\rho_q\mu_q)^{1/2}} + \frac{f_0^{3/2}(\rho\eta)^{1/2}}{(\pi\rho_q\mu_q)^{1/2}}\left[\frac{a(a+1)}{(1+a)^2+a^2}\right] \tag{28}$$

$$\Delta\Gamma - \Delta\Gamma_l = -\frac{2f_0^{3/2}(\rho\eta)^{1/2}}{(\pi\rho_q\mu_q)^{1/2}}\frac{a^2}{(1+a)^2+a^2}. \tag{29}$$

Equation 28 shows that there are two different contributions to the frequency shift, Δf_m and Δf_{sl}, which originate from: (i) a change of the mass of the adsorbed layer rigidly coupled to the surface (first term on the right hand side of Eq. 28), and (ii) partial decoupling between the quartz crystal oscillations and the solution, caused by slippage at the adsorbate–liquid interface (second term on the right hand side of Eq. 28). It should be stressed here that, in contrast to adsorption from the gas phase, adsorption from liquid phase can result in either a decrease or an increase of the resonant frequency, depending on its effect on the mass of the layer rigidly coupled to the surface and on changes of the coefficient of sliding friction, χ, which determined the slip length, according to Eq. 22.

Consider the effect of adsorption on the parameters Δm_a and χ. The layer adsorbed at the electrode–electrolyte interface contains two types of molecules: adsorbate and solvent. In the framework of mean field approximation, the effective interaction between the liquid and the adsorbed layer can be characterized by the energy $\varepsilon_{ls} \approx \varepsilon_{la}\boldsymbol{\Gamma}_a/\boldsymbol{\Gamma}_m + \varepsilon_{ll}(1 - \boldsymbol{\Gamma}_a/\boldsymbol{\Gamma}_m)$, where ε_{la} is the characteristic energy of the adsorbate–liquid interaction $\boldsymbol{\Gamma}_a$ and $\boldsymbol{\Gamma}_m$ are the surface excess and the maximum surface excess of the adsorbate, respectively. As a result, the slip length at the adsorbed layer–liquid interface can be

expressed as

$$b_s = f[(\varepsilon_{la}/\varepsilon_{ll})\boldsymbol{\Gamma}_a/\boldsymbol{\Gamma}_m + (1 - \boldsymbol{\Gamma}_a/\boldsymbol{\Gamma}_m)] \approx f(\varepsilon_{la}/\varepsilon_{ll})\boldsymbol{\Gamma}_a/\boldsymbol{\Gamma}_m\,, \tag{30}$$

showing an increase of b_s with $\boldsymbol{\Gamma}_a$ for $\varepsilon_{la}/\varepsilon_{ll} < 1$. Equation 30 is the interpolation formula that describes correctly the behavior of b_s for small $\boldsymbol{\Gamma}_a/\boldsymbol{\Gamma}_m$ and for $\boldsymbol{\Gamma}_a/\boldsymbol{\Gamma}_m = 1$. We note that, when the liquid and the adsorbate molecules are of significantly different size, the incommensurability between the structures of the adsorbed layer and the liquid grows with $\boldsymbol{\Gamma}_a$, which may lead to an additional enhancement of the slip length. What is important here is a relation between scales of corrugations of the potential energy in the solvent and the adsorbate molecules, rather than their physical size.

The foregoing discussion shows that for $\varepsilon_{la}/\varepsilon_{ll} < 1$ the parameter $a = b_s/\delta$, in Eqs. 28 and 29, characterizing the effect of slippage on the response of the QCM increases with $\boldsymbol{\Gamma}_a$. For instance, for $\varepsilon_{la}/\varepsilon_{ll} \approx 0.5$, it may reach values as high as $a \approx 10^{-2}$, for $\boldsymbol{\Gamma}_a \approx \boldsymbol{\Gamma}_m$. Correspondingly, the adsorption-induced slippage leads to a positive frequency shift, which grows with $\boldsymbol{\Gamma}_a$. This contribution can be larger than the effect of added weight. As a result, the overall frequency shift due to adsorption can be positive and increases with $\boldsymbol{\Gamma}_a$ [61]. It should be noted that, for small values of the parameter a, the effect of slippage on the resonance frequency shift is much larger than its effect on the width of the resonance (Eqs. 28 and 29). Also, slippage will always cause a decrease in the width of the resonance. Thus, if a positive shift of frequency with adsorption is to be associated with enhanced slippage, it should also be exhibited as a reduction of the width of the resonance, although the latter may be hard to detect experimentally.

The approach described above has been applied to treat experimental data on adsorption of pyridine from the electrolyte solutions [61]. Using Eq. 28 made it possible to determine the slip length as a function of surface excesses of pyridine. In agreement with the theoretical prediction, it was found that b_s grows with $\boldsymbol{\Gamma}_a$. The values of b_s did not exceed 0.3 nm and 1.2 nm for adsorption from butanol and water solutions, respectively. The dependence of slip length on surface excess was essentially linear (Eq. 30) for pyridine adsorption from butanol solution, but deviated from linearity for pyridine adsorption from water. The deviation was attributed to a reorientation of adsorbed pyridine molecules at the Au surface.

Above, we discussed the situation where the adsorbed layer is rigidly attached to the oscillating crystal surface, and there is finite slippage at the adsorbate–liquid interface. An alternative model, based on the assumption that slippage occurs at the crystal-adsorbed interface and non-slip boundary conditions apply to the adsorbate–liquid interface, can also be considered. For a small slip length, $b_s \ll \delta$, this model leads to the same results for the shift of the complex resonance frequency as the model discussed above and measurements employing the QCM cannot distinguish between them. How-

ever, in the case of specific adsorption, the assumption of slippage at the crystal-adsorbed layer interface is hard to justify, since the characteristic energy of adsorbate–substrate interactions, ε_{as}, is larger than the energy of adsorbate–adsorbate interactions, ε_{aa}, hence the corresponding slip length $b_s = f(\varepsilon_{as}/\varepsilon_{aa})$ is expected to be very small.

4
Quartz Crystals with Rough Surfaces Operating in Liquids

4.1
Theoretical Approaches

When the surface of a quartz crystal resonator is rough, the liquid motion generated by the oscillating surface becomes much more complicated than for the smooth surface. A variety of additional mechanisms of coupling between the acoustic waves in the solid and the motion in the liquid can arise. These may include generation of non-laminar motion, the conversion of in-plane surface motion to motion normal to the surface, and trapping of liquid by cavities and pores. It has been experimentally demonstrated [14, 17, 75–79] that the roughness-induced response of the QCM includes both the inertial and viscous contributions. Measurements of the complex shear mechanical impedance [14] were used to analyze different contributions to the roughness-induced response of the quartz resonator, and to correlate the experimental results with the surface roughness of the quartz resonator. Nevertheless, this subject is poorly developed, and the interpretation of experimental results can often be ambiguous.

The dependence of the QCM response on the morphology of the interface is determined by the relation between the characteristic sizes of roughness and the length scales of the shear modes in the liquid and the quartz resonator. The length scales in the liquid (the velocity decay length, δ) and in the crystal (wave length of the shear-mode oscillations, λ_q) are defined by the Navier–Stokes equation and by the wave equation for elastic displacement, respectively. For typical frequencies used in QCM experiments, $f_0 \approx 5$–10 MHz, the lengths $\delta = (\eta/\pi f_0 \rho)^{1/2}$ and $\lambda_q = (\mu_q/\rho_q)^{1/2} f_0^{-1}$ are of the order 0.177–0.25 μm and 0.03–0.1 cm, respectively.

The surface profile may be specified by a single valued function $z = \xi(\boldsymbol{R})$ of the lateral coordinates $\boldsymbol{R}$ that defines a local height of the surface with respect to a reference plane ($z = 0$). The latter is chosen so that the average value of $\xi(\boldsymbol{R})$ will equal zero. Surfaces used in QCM experiments may have various scales of roughness. In order to clarify this point, let us consider the two limiting cases: *slight* and *strong* roughness structures, which are schematically shown in Fig. 3. For the slight roughness (Fig. 3a) the "amplitude" of deviation from the reference plane $z = 0$ is much less than the lateral charac-

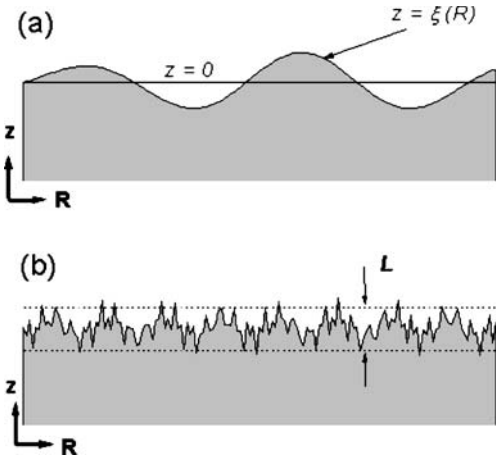

Fig. 3 Schematic representation of a slight (**a**) and a strong (**b**) roughness. The profile of slight roughness is described by the function $z = \xi(\boldsymbol{R})$. L is the effective thickness of the "porous" film that represents strong roughness. (From [27])

teristic length. In the case of strong roughness (Fig. 3b), the "amplitude" and "period" of repetitions are of the same order of magnitude.

In order to stress the multiscale nature of roughness, the profile function can be written as the sum of the functions that characterize the profile of the specific scale i:

$$\xi(\boldsymbol{R}) = \sum_i \xi_i(\boldsymbol{R}) \,. \tag{31}$$

For the calculation of the response of the QCM, the height–height pair correlation function is needed [80]. When rough structures having different scales do not correlate, the total correlation function can be written in the form:

$$\langle \xi(\boldsymbol{R}')\xi(\boldsymbol{R}' - \boldsymbol{R})\rangle = \sum_i \langle \xi_i(\boldsymbol{R}')\xi_i(\boldsymbol{R}' - \boldsymbol{R})\rangle \,, \tag{32}$$

where $\langle \xi_i(\boldsymbol{R}')\xi_i(\boldsymbol{R}' - \boldsymbol{R})\rangle$ is the correlation function for the scale i and $\langle \quad \rangle$ means averaging over the lateral coordinates. Usually one assumes that the correlation function $\langle \xi_i(\boldsymbol{R}')\xi_i(\boldsymbol{R}' - \boldsymbol{R})\rangle$ has a Gaussian form $\langle \xi_i(\boldsymbol{R}')\xi_i(\boldsymbol{R}' - \boldsymbol{R})\rangle = h_i^2 \exp(-|\boldsymbol{R}|^2 / l_i^2)$, where h_i is the root mean square height of the roughness and l_i is the lateral correlation length, which represents the lateral scale. Thus, the morphology of the rough surface can be characterized by a set of lengths [81].

It is impossible at the present time to provide a unified description of the response of the QCM for non-uniform solid–liquid interfaces with arbitrary geometrical structure. Below we summarize results obtained for the limiting cases of slight and strong roughness.

4.1.1 Slight Roughness

For slightly rough surfaces, the problem was solved in the framework of perturbation theory with respect to the parameters $|\nabla\xi(\boldsymbol{R})| \ll 1$ and $h/\delta \ll 1$, where h is the root mean square height of the electrode surface [80, 82]. The first condition means that the local slope of the interface is small, i.e., the height, h, is less than the lateral characteristic length (i.e., the correlation length, l) of the roughness.

For roughness described by a one-scale correlation function, the shift in the resonant frequency and the half-width of the resonance can be written in the following form [80, 82]:

$$\Delta f = -\frac{f_0^2\rho\delta}{(\rho_q\mu_q)^{1/2}}\left[1+\frac{h^2}{l^2}F(l/\delta)\right] \tag{33}$$

$$\Delta\Gamma = \frac{f_0^2\rho\delta}{(\rho_q\mu_q)^{1/2}}\left[1+\frac{h^2}{l^2}\Phi(l/\delta)\right]. \tag{34}$$

The scaling functions $F(l/\delta)$ and $\Phi(l/\delta)$ are expressed through the Fourier components of the height–height correlation function of the roughness $g(\boldsymbol{K})$ [82], which can be defined as:

$$h^2 g(\boldsymbol{K}) = \int \mathrm{d}\boldsymbol{R}\exp(-i\boldsymbol{K}\boldsymbol{R})\langle\xi(\boldsymbol{R}')\xi(\boldsymbol{R}'-\boldsymbol{R})\rangle\,. \tag{35}$$

The correlation function provides the most detailed characterization of the surface structure. Sometimes the surface roughness is described by an integral parameter, the roughness factor, R, which is the ratio between the true and the apparent (geometrical) surface area. For slight roughness, the roughness factor is expressed through the correlation function [82] as:

$$R = 1+\frac{h^2}{2}\int\frac{\mathrm{d}\boldsymbol{K}}{(2\pi)^2}g(\boldsymbol{K})K^2\,. \tag{36}$$

For the Gaussian random roughness $g(\boldsymbol{K}) = \pi l^2\exp(-l^2K^2/4)$ and Eq. 36 yield $R = 1+2h^2/l^2$.

It should be noted that the roughness factor, R, relevant to the operation of the QCM is not the same as the roughness factor commonly referred to in studies of adsorption and interfacial electrochemistry, because of the difference in corresponding length scales. The QCM roughness factor is mostly determined by the roughness on the scale of the velocity decay length in the liquid, δ, which assumes values of hundreds of nanometers, depending on the frequency of the crystal and the viscosity and density of the liquid. The "interfacial" roughness factor is related to the structure of the molecular adsorbed layer, or the double layer, or to the charge transfer at the interface, and therefore its characteristic scale is about 1 nm.

The first terms in braces in Eqs. 33 and 34 define the shift and the broadening of the resonance at the interface between an ideally smooth crystal and the liquid [13]. The surface roughness leads to an additional decrease of the resonant frequency and a broadening of the half-width of the resonance, expressed by the second terms in this equation.

The particular form of the scaling functions $F(l/\delta)$ and $\Phi(l/\delta)$ is determined by the morphology of the surface. However, the asymptotic behavior of these functions for $l/\delta \gg 1$ and $l/\delta \ll 1$ is universal [82] and has the form:

$$F(l/\delta) = (l/\delta)[\alpha_1 + \alpha_2\delta/l] \quad \text{at} \quad l/\delta \gg 1 \tag{37}$$

$$F(l/\delta) = (l/\delta)[\beta_1 + \beta_2 l/\delta] \quad \text{at} \quad l/\delta \ll 1 \tag{38}$$

$$\Phi(l/\delta) = \gamma_1 \quad \text{at} \quad l/\delta \gg 1 \tag{39}$$

$$\Phi(l/\delta) = (l/\delta)^2\gamma_2 \quad \text{at} \quad l/\delta \ll 1\,. \tag{40}$$

For random Gaussian roughness, the parameters are:

$$\alpha_1 = \pi^{1/2}, \alpha_2 = 2, \beta_1 = 3\pi^{1/2}, \beta_2 = -2 \quad \text{and} \quad \gamma_1 = \gamma_2 = 2\,. \tag{41}$$

It should be noted that for $l/\delta \gg 1$ the roughness-induced frequency shift includes a term that does not depend on the viscosity of the liquid, the first term in Eqs. 37 and 33. It reflects the effect of the non-uniform pressure distribution, which is developed in the liquid under the influence of a rough oscillating surface [80]. The corresponding contribution has the form of the Sauerbrey equation. This effect does not exist for smooth interfaces. The second term in Eq. 37 and Eq. 39 describe a viscous contribution to the QCM response. Their contribution to Δf has the form of the QCM response at a smooth liquid–solid interface, but includes an additional factor R that is a roughness factor of the surface. The latter is a consequence of the fact that for $l/\delta \gg 1$ the liquid "sees" the interface as being locally flat, but with R times its apparent surface area.

Results obtained in [80, 82] show that the influence of slight surface roughness on the frequency shift cannot be explained in terms of the mass of liquid "trapped" by surface cavities, as proposed in [76, 77]. This statement can be illustrated by consideration of the sinusoidal roughness profile. The mass of the liquid "trapped" by sinusoidal grooves does not depend on the slope of the roughness, h/l, and is equal to $S*h$, where S is the area of the crystal. However, Eq. 33 demonstrates that the roughness-induced frequency shift does increases with increasing slope.

Equation 34 and the asymptotic behavior of the scaling functions show that in the regions where $l/\delta \gg 1$ and $l/\delta \ll 1$, the width is proportional to the factors $(\rho\eta)^{1/2}f_0^{3/2}$ and $\rho^{3/2}\eta^{-1/2}f_0^{5/2}$, respectively. In the high viscosity limit, when $\eta > l^2\pi\rho f_0$, the roughness-induced frequency shift approaches a constant value and the roughness-induced width tends to zero.

The results obtained make it possible to estimate the effect of roughness on the response of the QCM, if the surface profiles function $\xi(\boldsymbol{R})$ can be found from independent measurements.

4.1.2 Strong Roughness

Perturbation theory cannot be applied to describe the effect of the strong roughness. An approach based on Brinkman's equation has been used instead to describe the hydrodynamics in the interfacial region [83]. The flow of a liquid through a non-uniform surface layer has been treated as the flow of a liquid through a porous medium [84–86]. The morphology of the interfacial layer of thickness, L, has been characterized by a local permeability, ξ_{H}, that depends on the effective porosity of the layer, ϕ. A number of equations for the permeability have been suggested. For instance, the empirical Kozeny–Carman equation [84] yields a relationship between ξ_{H}^2 and the effective porosity $\xi_{\mathrm{H}}^2 \sim r^2\phi^3/(1-\phi)^2$, where r is the characteristic size of inhomogeneities.

The flow of liquid through the interfacial layer can be described by the following equation [83]:

$$i\omega\rho v(z,\omega) = \eta\frac{\mathrm{d}^2}{\mathrm{d}z^2}v(z,\omega) + \eta\xi_{\mathrm{H}}^{-2}[v_{\mathrm{q0}} - v(z,\omega)]\,, \tag{42}$$

where v_{q0} is the amplitude of the quartz surface velocity and $v(z,t) = v(z,\omega)\exp(i\omega t)$ is the velocity of the liquid in the layer. In this equation the effect of the solid phase on the flow of liquid is given by the resistive force, which has a Darcy-like form, $\eta\xi_{\mathrm{H}}^{-2}[v_{\mathrm{q0}} - v(z,\omega)]$. In the case of high effective porosity, the resistive force is small and Eq. 47 is reduced to the Navier–Stokes equation, describing the motion of the liquid in contact with a smooth quartz surface. For a given viscosity, the resistive force increases with decreasing effective porosity and strongly influences the liquid motion. At very low effective porosity all the liquid located in the layer is trapped by the roughness and moves with a velocity equal to the velocity of the crystal surface itself.

Brinkman's equation represents a variant of the effective medium approximation, which does not describe explicitly the generation of non-laminar liquid motion and conversion of the in-plane surface motion into the normal-to-interface liquid motion. These effects result in additional channels of energy dissipation, which are effectively included in the model by introduction of the Darcy-like resistive force.

The liquid-induced frequency shift and the half-width of the resonance have the following form [83]

$$\Delta f = -\frac{2f_0^2\rho}{(\mu_q\rho_q)^{1/2}} \times \mathrm{Re}\left\{\frac{1}{q_0} + \frac{L}{\xi_H^2 q_1^2} - \frac{1}{W}\frac{1}{\xi_H^2 q_1^2}\left[\frac{2q_0}{q_1}[\cosh(q_1 L) - 1] + \sinh(q_1 L)\right]\right\} \tag{43}$$

$$\Delta\Gamma = -\frac{2f_0^2\rho}{(\mu_q\rho_q)^{1/2}} \times \mathrm{Im}\left\{\frac{1}{q_0} + \frac{L}{\xi_H^2 q_1^2} - \frac{1}{W}\frac{1}{\xi_H^2 q_1^2}\left[\frac{2q_0}{q_1}[\cosh(q_1 L) - 1] + \sinh(q_1 L)\right]\right\} . \tag{44}$$

Here $q_0 = (i2\pi f_0\rho/\eta)^{1/2}$, $q_1^2 = q_0^2 + \xi_H^{-2}$, and $W = q_1\cosh(q_1 L) + q_0\sinh(q_1 L)$. The first terms on the right-hand sides of Eqs. 43 and 44 describe the response of the QCM for the smooth quartz crystal–liquid interface [13]. The additional terms present the shift and the half-width of the QCM response caused by the interaction of the liquid with a non-uniform interfacial layer.

When the permeability length scale is the shortest length of the problem, $\xi_H \ll \delta$ and $\xi_H \ll L$, the layer-induced shift, Δf_L, is proportional to the density of the liquid and does not depend on the viscosity. It has the form of the Sauerbrey equation for mass loading. This effect results from the inertial motion of the liquid trapped by the inhomogeneities in the interfacial layer.

$$\Delta f_L = -\frac{2f_0^2\rho}{(\mu_q\rho_q)^{1/2}}(L - \xi_H) . \tag{45}$$

The effective thickness of the liquid film rigidly attached to the oscillating surface is equal to $L - \xi_H$, and is less than the thickness of the inhomogeneous layer, L. The increase of the permeability ξ_H leads to the enhancement of the velocity gradient in the layer, which results in a decrease of the shift due to mass loading, and an increase of the width caused by the energy dissipation. When the layer thickness is the shortest length of the problem, $L \ll \delta$, $L \ll \xi_H$, and $\xi_H \ll \delta$, the frequency shift is also proportional to the density of the liquid and does not depend on viscosity:

$$\Delta f_L = -\frac{2f_0^2\rho L}{3(\mu_q\rho_q)^{1/2}}(L/\xi_H)^2 . \tag{46}$$

However, in contrast to the previous case, it cannot be related to the mass of trapped liquid. The correction to the width of the resonance depends on the viscosity and is substantially less than the layer-induced shift.

4.2 Experimental Studies

4.2.1 Non-conducting Liquids

Experimentally, correlation between the QCM signal and the surface morphology, as determined by microprofilometry and STM techniques, has already been established in the early experiments with the QCM in liquids [14, 16]. Measurements indicated that the mechanical impedance, Z_L, increases with increasing surface roughness. In contrast to smooth surfaces, interactions of rough oscillating surfaces with liquids do not contribute equally to $\mathrm{Re}(Z_L)$ and $\mathrm{Im}(Z_L)$ [14, 87, 88]. It was also found that the roughness leads to new dependencies of the frequency shift on viscosity, which does not appear for smooth surfaces. For instance, the experimental data obtained in methanol–water mixtures and in alcohols [16] demonstrated that the effect of roughness on the QCM is most pronounced for low viscosities, where the liquid-induced shift of the resonance frequency is small. This conclusion agrees with the theoretical predictions discussed in Sect. 4.1 (see Eqs. 33 and 34). Theory shows that, at low viscosities, the QCM response in liquids is mainly determined by the contribution of the non-uniform pressure distribution, which is developed in the liquid under the influence of a rough oscillating surface [89].

In [27] experiments in liquids having a wide range of viscosity and density were performed, and the response of the QCM was analyzed, using the theoretical models described in Sect. 4.1. Both parameters characterizing the resonator, the shift in fundamental frequency and the width of the resonance, were measured simultaneously. The usual form of presenting the experimental data in liquids is to plot the real and the imaginary components of the response of the QCM as a function of the density of the liquid or of the parameter $\sqrt{\rho\eta}$. However, these parameters are the natural variables only for ideally flat interfaces. Equations 33, 34, 43 and 44 show that for rough surfaces it is more convenient to consider the quantities $\Delta\Gamma/f^2\rho$ and $\Delta f/f^2\rho$, as a function of the velocity decay length in the liquid, δ, as shown in Fig. 4. The dependence of these two parameters on δ is linear for the ideally smooth surface of the quartz crystal resonator loaded on one side, (see line 1 in Fig. 4a,b).

Close points in these figures represent data measured on a relatively smooth surface, (obtained by vacuum sputtering), while open points were taken on a surface with strong roughness, prepared by electroplating. The deviation of the data from the straight line 1 calculated for an ideally smooth surface increases with increasing roughness, as expected.

The experimental dependence of the quantity $\Delta\Gamma/f^2\rho$ on the velocity decay length exhibits a sharp increase at low values of δ, followed by a gentle growth at large values of δ. This effect becomes more pronounced with increasing roughness (open circles).

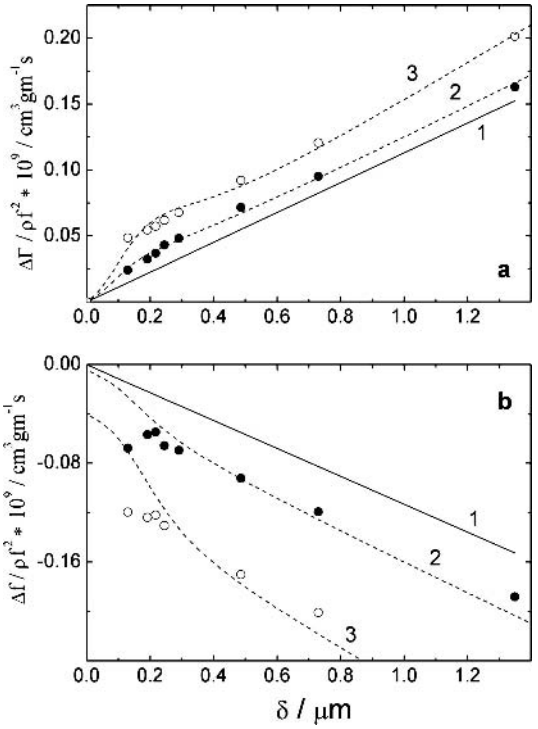

Fig. 4 Dependence **a** of the parameter $\Delta\Gamma/\rho f^2$ and **b** $\Delta f/\rho f^2$ on the velocity decay length in different liquids, for an ideally smooth surface (*lines 1*), and experimental data for two real surfaces: vacuum-sputtered gold (*closed circles*) and electrochemically deposited gold (*open circles*). *Lines 2* and *3* represent results of parameter fitting, see text. (From [27])

In Fig. 5a, the theoretical dependence of the function $\Delta\Gamma/f^2\rho$ on δ is given (lines 2–4) for different values of the local permeability, ξ_H, and a fixed value of the film thickness parameter, L, in the framework of the theory developed for strong roughness (Sect. 4.1.2). At large values of δ, the calculated lines approach line 1 for an ideally smooth surface. This behavior can be understood since it becomes difficult for the liquid to move inside pores in the surface film when δ is much larger than the size of the pores. In the limiting case the liquid moves in-phase with the solid surface, acting only as a mass loading, but adding nothing to the width of the resonance.

Line 5 in Fig. 5 is calculated for a surface having slight roughness, according to Eq. 34 and 39. The hydrodynamic roughness factor R is chosen so that this line connects the origin with the experimental point for the highest value of δ. This yielded a value of $R = 1.3$.

Curves 2–4 in Fig. 5b were calculated for different values of the film thickness, L, and a constant value of the local permeability, ξ_H, according to Eq. 44.

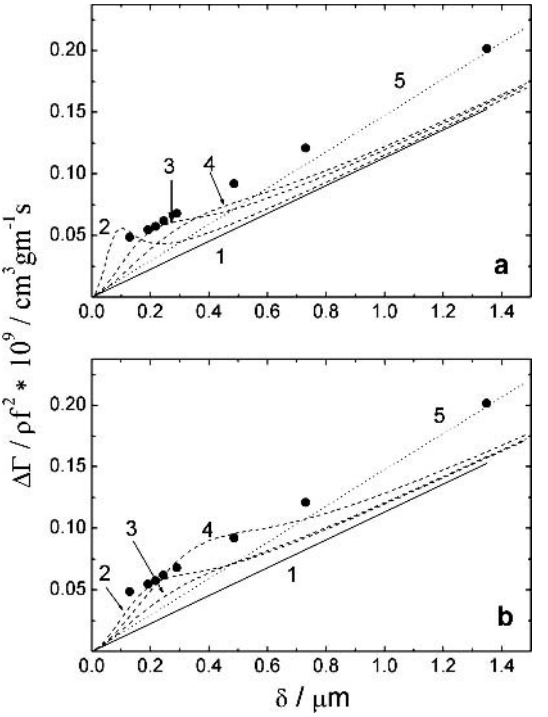

Fig. 5 Dependence of the parameter $\Delta\Gamma/\rho f^2$ on the velocity decay length: *points* experimental data, *line 1* in both plots indicates an ideally smooth surface. **a** Influence of strong roughness according to Eq. 44 for different values of ξ_H: *2* 69, *3* 172, *4* 276 nm) and $L = 506$ nm. **b** The same for different values of L: *2* 460, *3* 506, *4* 690 nm and $\xi_H = 172$ nm. *Line 5* in both plots was calculated for slight roughness (roughness factor $R = 1.3$, Eqs. 34 and 39). (From [27])

Lines 1 and 5 are the same as in Fig. 5a. The width of the resonance is seen to increase with increasing film thickness.

Figure 5 shows that there is no way to fit the experimental data assuming that only one type of roughness is presented on the surface. We are thus forced to conclude that, in these experiments the surface has a multiscale roughness, shown schematically in Fig. 6. The structure of this rough surface is a combination of a slight and a strong roughness shown in Fig. 3a,b. When this is taken into account, it is possible to use Eqs. 33, 34, 43, and 44 to calculate the shift in resonance frequency and shift in the width of the resonance, and fit the experiments to the calculated curves with properly chosen values of the parameters of strong roughness. The result of such a fit is shown in Fig. 4, curves 2 and 3. For details of the fitting procedure, the limitations associated with the use of a simplified model, and the comparison with STM data see [27].

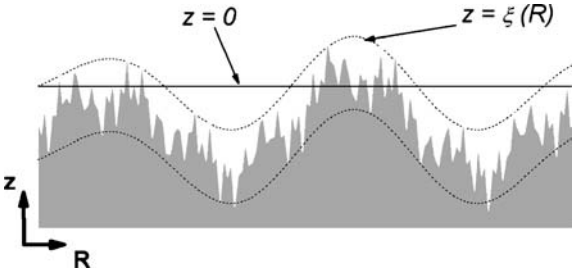

Fig. 6 Schematic representation of multiscale roughness. This structure is a combination of a slight and a strong roughness shown in Fig. 3a,b. (From [27])

Here we should emphasize only one point, of major importance for electrochemical use of the QCM. The velocity decay length of most solvents of interest for electrochemical and analytical purposes happen to be at the lower end of the values of δ shown in Figs. 4 and 5. This is the region where the interplay between the two types of roughness is the strongest, and it is the most difficult to fit the data to either model. This inherent difficulty should be borne in mind whenever an attempt is made to interpret the impedance response of the QCM operating in typical solvents such as water, alcohols, or many of the other non-aqueous solvents employed in electrochemistry.

The importance of measuring the imaginary component of the quartz crystal in order to study metal deposition and dissolution processes has also been noted by the authors of [26, 88]. In particularly, in this way they [26] succeeded in separating contributions of mass loading and roughness to QCM response and to characterize the electrode roughness.

Recently it has been suggested that shear oscillations of rough surfaces can generate acoustic compressional waves in the liquid at the second harmonic frequency if the amplitude of oscillations is large enough [90, 91]. This effect has been detected while electrochemically growing a rough metal surface on the QCM device. It should be noted that mass loading, viscosity, and slippage effect do not contribute to the second harmonic generation, and thus the second harmonic generation would allow for an independent measurement of the surface roughness with the QCM technique. Unfortunately under realistic conditions, the acoustic signal at the second harmonic frequency is too small to obtain quantitative results.

4.2.2 The Electrochemical Case

There are only few publications where the response of the QCM in electrochemical systems has been studied on intentionally roughened surfaces [25,

26, 92–95]. Figure 7 shows how the response of the EQCM changes with the change of surface roughness, induced by extensive cycling into the region of surface oxide formation. When the surface was not roughened, the loops de-

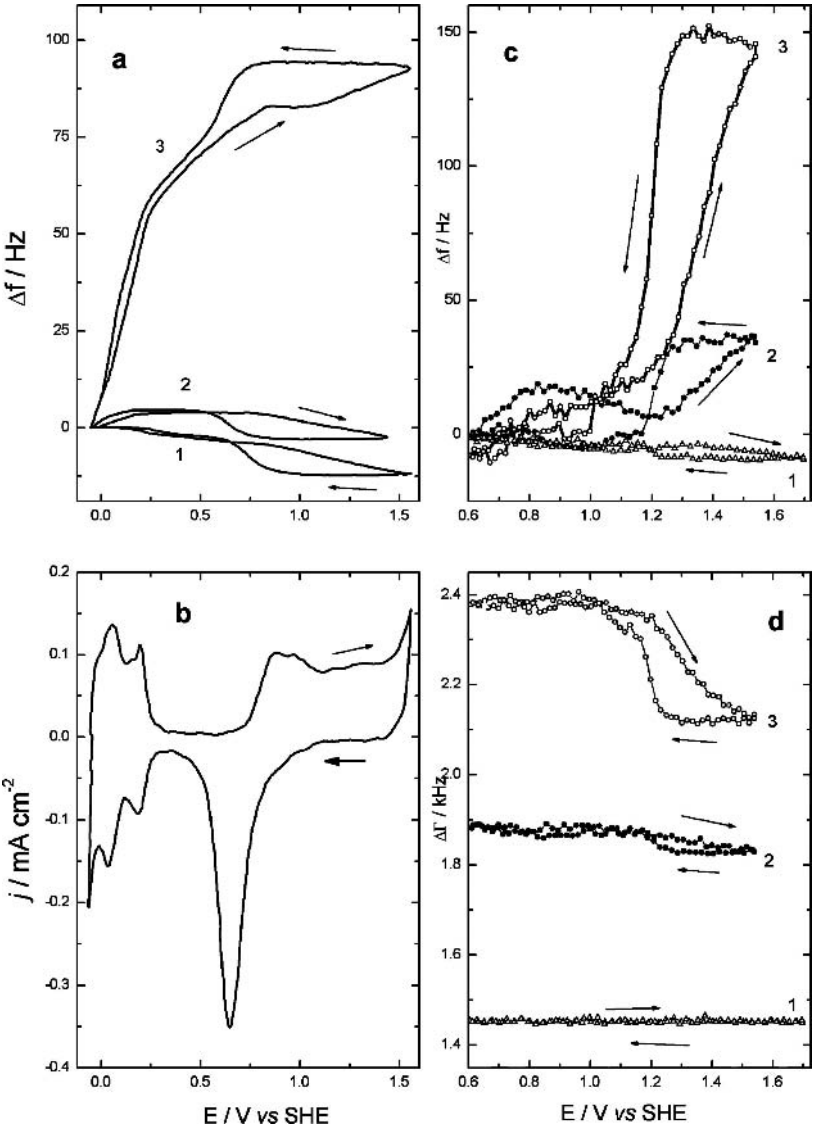

Fig. 7 **a** Influence of the number of oxidation–reduction cycles on the frequency response for platinum in 0.2 M H_2SO_4, at 100 mV/sec (*curve 1* 100, *2* 2000, *3* 10 000 cycles). **b** Stabilized cycling voltammogram for Pt electrode. **c** Frequency shift and **d** width of resonance for gold electrodes in 0.1 M $HClO_4$ at 10 mV/sec (*curve 1* 4, *2* 100, *3* 500 cycles). (**a** and **b** from [93])

scribing the shift in frequency with potential, associated with surface oxide formation, have clockwise directions, (see curves 1 in Fig. 7a,c). On very rough surfaces, (represented by curves 3), the loops are in the opposite direction. The data for platinum electrode (Fig. 7a,b) were taken from [93], in which only the shift of resonance frequency was measured. The data on the gold electrode were obtained in our own laboratory, and both the shift of frequency and the width of the resonance were measured (Fig. 7c,d). The latter shows that when the surface is sufficiently smooth there are no changes in the width of resonance with the potential. The corresponding curves for rough surfaces, when the resonance is wide ($\Delta\Gamma > 1.5$ kHz), show strong potential dependence and remarkable hysteresis. On the one hand the comparison of voltammograms and dependence of the responses of the EQCM on potential clearly shows that the hysteresis is associated with surface oxide formation. On the other hand, the effect cannot be ascribed to mass loading because the frequency shift on rough surfaces is not only larger than that on smooth surfaces – the effect has a reverse sign. Moreover, mass loading alone cannot lead to changes in $\Delta\Gamma$. The loop of frequency shift also changes its sign in the region of hydrogen adsorption on platinum. It should be noted that the surface of Pt is much more resistant to roughening than that of gold. Thus, comparing Figs. 7a,c it would seem that cycling 2000 and 10 000 times on Pt has an effect comparable to that of cycling Au 100 and 500 times, respectively. However, the experiments on Pt and Au shown they were performed under similar, but not identical, conditions.

Comparison of Fig. 7c,d for a highly rough surface (curve 3) shows that a decrease in width is associated with a positive shift in resonance frequency, in the region of surface oxide formation. This is consistent with the notion that both effects result from a weakening of the interactions between the vibrating surface and the liquid under surface oxidation. Similar results have been obtained for gold surfaces having different degrees of roughness.

All the data obtained with rough surfaces and the discussion of these data [25, 28, 92, 93, 95] lead to the following conclusions

1. The roughness of the electrode has a profound influence on the response of the EQCM, see Figs. 7 and 8. This may explain the unusually large discrepancies among data obtained with the EQCM in different laboratories (not necessarily on intentionally roughened surfaces). A good example is the large discrepancy in data reported for the region of surface oxide formation on gold [76, 96–100].
2. The response of the EQCM on rough surfaces cannot be treated in terms of the electrochemically defined roughness factor $\tilde{R}$, which is obtained from adsorption phenomena, e.g., from data such as presented in Fig. 9. This quantity can be considered as representing all adsorption sites on the surface, which is equivalent to the surface roughness on the atomic scale. However, the response of the EQCM depends on roughness on a meso-

scopic scale, which is comparable to the hydrodynamic velocity decay length rather than to the double layer thickness.

3. The width of the resonance is an important characteristic of the surface, as seen in Fig. 8b, and can serve as a semi-quantitative measure of its roughness, on the scale relevant to the response of the EQCM. Unfortunately, only very few publication so far contain this information.

In addition to the conclusions drawn above, one is still left with the need to interpret the dependence of the response of the EQCM on potential on rough surfaces (Figs. 7 and 8). Attempts to provide a qualitative interpretation were made in [95, 101]. The authors ascribed the effects on rough surfaces to "formation of a structured region of solvent which leads to increased viscosity and consequent frequency changes" and agreed that "the exact nature of the changes in the surface ... still has to be established" [95]. Thus, they assumed that the properties of that "structured region of solvent" near the electrode depend on adsorption and on potential.

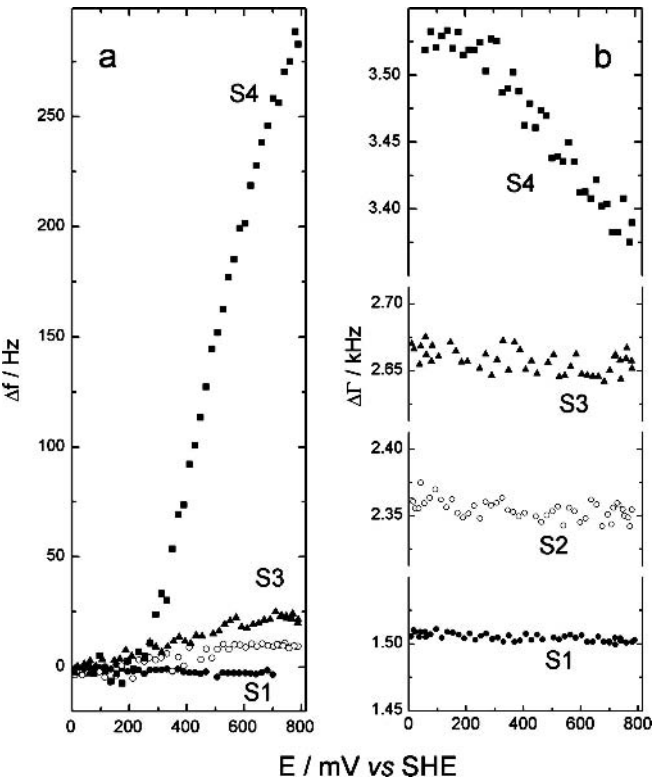

Fig. 8 Dependence of the frequency shift (**a**) and the half-width of the resonance (**b**) of the EQCM on potential, for different gold surfaces, *S1–S4* [28]. (From [28])

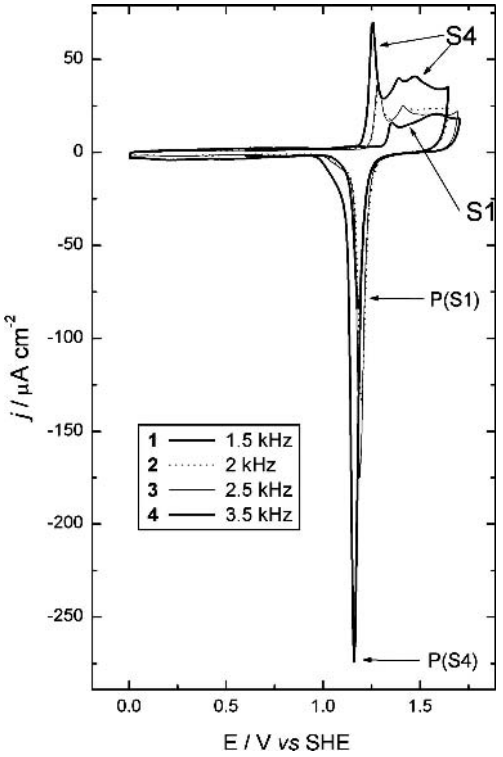

Fig. 9 Cycling voltammetry (5 mV/sec) for gold electrodes of different roughness [28]. *S1* untreated (as received) surface. *S2–S4* surfaces obtained by electrodeposition of gold at currents densities close to the limiting current density. *Inset*: approximate values of the half-width of resonance. *Curves S2* and *S3* lie between *curves S1* and *S4*, in some parts coinciding with them. *Arrows P(S1)* and *P(S4)*, show the peak currents for reduction of the surface oxide, measured for the surfaces *S1* and *S4*, respectively. (From [28])

5
Slippage at Rough Surfaces

Mesoscopic roughness at the solid–liquid interface can greatly modify both interfacial flow and static wetting properties leading to two behaviors, either a decrease [45, 64, 102] or an increase [63, 103] of surface slippage with roughness.

The calculations, which have been made for periodic and random surfaces [6, 104–106], demonstrated that if the liquid fully wets the solid surface, the roughness reduces slip and shifts the position of the effective surface plane (the plane where the liquid and substrate velocities are equal) in the direction of the liquid phase [6, 107]. The authors of [39, 108] suggested intro-

duction of an effective slip length, b_s^{eff}, which takes into account both slippage and roughness, in order to describe an interplay between the slippage and roughness. In this manner, liquid flow at a rough surface has been simulated as a flow at a smooth surface with an effective slip length. Application of this approach to the QCM problem [6] yields the following equation for the effective slip length:

$$b_s^{eff} = b_s \left\{ 1 - \left(\frac{h_0 k_0}{2} \right)^2 \left[\frac{3 + 4 b_s k_0}{1 + 2 b_s k_0} \right] \right\} - \frac{k_0 h_0^2}{2} \left[\frac{2 + 3 b_s k_0}{(1 + b_s k_0)(1 + 2 b_s k_0)} \right] . \tag{47}$$

Equation 47 was derived for a sinusoidal profile of roughness, $z(x) = d + h_0 \sin(k_0 x)$, with an amplitude h_0 and a period of $2\pi/k_0$, assuming that the decay length, δ, is the largest characteristic length of the problem, $\delta/b_s \gg 1$ and $\delta k_0 \gg 1$. Beyond these conditions the effective slip length is a complex function. Equation 47 shows that roughness diminishes the influence of slippage on the QCM response, namely the effective slip length becomes smaller than the corresponding length for the smooth interface. At rough interfaces, the effective slip length decreases with an increase of the amplitude of the surface corrugation and with a decrease of its period.

It should be noted that an effective slip length is not an intrinsic property of the surface. Its value depends also on the experimental configuration, for instance, b_s^{eff} found for the Poiseuille flow between rough surfaces [108] differs from the corresponding value obtained for QCM experiments (Eq. 47).

When the liquid partially wets the solid surface, roughness can lead to the spontaneous dewetting of a surface and the appearance of a superhydrophobic state, resulting in large slip length [103, 109, 110], and possibly in shear-rate-dependent effects [111]. It was also claimed that under these conditions roughness favors the formation of vapor or gas pockets (nanobubbles) trapped at the solid surface, which could be an important factor in slippage phenomena [55, 56]. It was proposed to simulate the effect of nanobubbles on the QCM signal through the introduction of laterally heterogeneous slip [112]. Over the last 5 years many groups have reported experimental observations of nanobubbles against hydrophobic surfaces in water [113–120]. The amount of slip has been observed experimentally to depend on the type and quantity of dissolved gas. However, there is great variation in published results and the observed behaviors are very sensitive to the surface preparation. The formation and stability of nanobubbles, even on hydrophobic surfaces, is not easily explained.

The formation of bubbles at solid surfaces has also been studied with the QCM technique. In [121] a non-linear dependence of $\Delta f/\rho$ on $(\eta\rho)^{0.5}$ was interpreted as the result of the presence of nanobubbles on the surface. However, it should be noted that the observed dependencies could be also explained using the concept of multiscale roughness discussed above (see

Sects. 4.1.2 and 4.2.1). In order to check the hypothesis of bubble formation, the authors of [122] immersed dry surfaces of the QCM of different roughness and hydrophobicity into electrolytes saturated by oxygen (or hydrogen). In all cases removing gases in situ by electrochemical reduction (or oxidation) did not result in changes of either the resonant frequency or the width of resonance. This led to a conclusion that even on freshly formed metal/aqueous solution contacts, the size and coverage of bubbles (if they exist) are so low that they could not influence the QCM response.

The above discussion shows that existing literature contains arguments, both theoretical and experimental, in favor as well as against the presence of nanobubbles at the metal/liquid interface. Many more targeted experiments and theoretical works are required to clarify this issue.

6 Conclusion

The quartz crystal resonator is a useful device for the study of thin-layer and interfacial phenomena. The crystals commonly employed have a fundamental resonance frequency of 5–10 MHz and a resolution of the order of 0.1–0.5 Hz. This high resolution makes the device sensitive to a myriad of physical phenomena, some of which are interrelated and some quite independent of each other. It cannot be overemphasized that the quartz crystal resonator acts as a true microbalance (more appropriately a nanobalance) only if in the course of the process being studied, the nature of the interface (its roughness, slippage, the density and viscosity of the solution adjacent to it, and the structure of the solvent in contact with it) is maintained constant.

In this chapter we have limited our discussion to the effects of interfacial structure on the QCM response in liquids.

Some of the main conclusions are listed below:

- The shift in frequency observed experimentally cannot be interpreted in terms of a change in mass loading alone, unless the conditions have been carefully chosen to ensure that this is the only factor affecting the resonance frequency.
- It seems to be essential to measure the admittance spectrum and determine both the resonant frequency shift and the width of the resonance simultaneously. This yields additional information not available from measurement of the resonant frequency alone, and can hence provides more detailed interpretation of processes occurring at the solid–liquid interface.
- Surface roughness is of paramount importance in the use of the QCM in liquids. The existing theories provide a description of the QCM response for rough surfaces in two limiting cases of slight and strong roughness. How-

ever, much is left to be developed for a quantitative interpretation of data obtained for real surfaces. In order to overcome the gap between existing theory and experiments, measurements on specially prepared surfaces with well-defined roughness should be performed.

- Numerous experimental techniques employed to study solid–liquid interfaces (X-ray and neutron scattering, optical, AFM and STM, adsorption, double layer capacitance, rotating disc electrode and QCM) are sensitive to the roughness of substrate surfaces. It should be noted that each technique probes roughness on the particular characteristic scale only, which is the atomic scale for X-ray and neutron scattering, AFM, STM, adsorption and double-layer capacitance measurements; a wave-length of light for optical measurements; the Nernst diffusion layer for rotating disc electrode experiments; and the hydrodynamic velocity decay length for the QCM. Thus, the impedance of the QCM would be expected to respond to roughness of about 10 nm and above, ignoring most of the so-called atomic scale roughness, but detecting roughness that can usually be ignored in experiments conducted under mass transport limitations.
- The results obtained by the QCM contain information relevant to the understanding of phenomena in the area of nanotribology, where techniques such as SFA and AFM are used. In both cases the results carry information regarding the properties of a nanoscale layer of liquid at the interface.
- An important part of modern experimental surface science and electrochemistry has been performed on single-crystal electrodes. In contrast, the metal deposited on the surface of the quartz resonator always has a rough surface and at best a preferred crystal orientation. Studies with a QCM having a true single crystal surface have not yet been reported. Making a thin (about 1 μm) stable single-crystal metal layer on the surface of quartz seems to be an insurmountable problem.

So far most of the QCM data were analyzed on a qualitative level only. The next step in QCM studies requires a quantitative treatment of the experimental results. The theoretical basis for the solution of this problem already exists, and has been discussed in this chapter. Joint experimental and theoretical efforts to elevate the QCM technique to a new level present a challenge for future investigators.

Finally it would seem that, in spite of some shortcomings, the potential advantages of the QCM far exceed its limitations. There are many challenges to overcome and the QCM will undoubtedly continue to be one of the important tools in studies of metal–solution interfaces in general.

Acknowledgements Financial support for this work by the Israel Science Foundation (grants No. 773/05 and 174/05) and by the Deutsche Forschungsgemeinschaft (HA 1517/26-1) is gratefully acknowledged. We thank Dr. G. Zilberman, and Mrs. G. Katz for their contribution in obtaining the experimental data discussed in this chapter.

References

1. Schumacher R (1990) Angew Chem Int Engl 29:329
2. Buttry DA (1991) Application of the quartz crystal microbalance to electrochemistry. In: Bard AJ (ed) Electroanalytical chemistry. Dekker, NY, p 1
3. Buttry DA (1991) The quartz crystal microbalance as an in situ tool in electrochemistry. In: Abruna HD (ed) Electrochemical interfaces – modern techniques for in situ interface characterization. Wiley, NY, p 531
4. Buttry DA, Ward MD (1992) Chem Rev 92:1355
5. Hepel M (1999) Electrode solution interface studied with electrochemical quartz crystal nanobalance. In: Wieckowski A (ed) Interfacial electrochemistry. Dekkker, NY, p 599
6. Tsionsky V, Daikhin L, Urbakh M, Gileadi E (2003) Looking at the metal/solution interface with the electrochemical quartz crystal microbalance. theory and experiment. In: Bard AJ, Rubinstein I (eds) Electroanalytical chemistry. Dekker, New York, p 1
7. Hillman AR (2003) The electrochemical quartz crystal microbalance. In: Bard AJ (ed) Encyclopedia of electrochemistry. Wiley, Weinheim, p 230
8. Sauerbrey G (1959) Z Phys 155:206
9. Moret H, Louwerix E (1966) Microbalance for ultrahigh-vacuum applications. In: Behrndt KHN (ed) Vacuum microbalance techniques. Plenum, NY, p 59
10. Tsionsky V, Gileadi E (1994) Langmuir 10:2830
11. Nomura T, Iijima M (1981) Anal Chim Acta 131:97
12. Bruckenstein S, Shay M (1985) Electrochim Acta 30:1295
13. Kanazawa KK, Gordon JG (1985) Anal Chim Acta 175:99
14. Martin SJ, Frey G, Ricco A, Senturia S (1993) Anal Chem 65:2910
15. Tsionsky V, Daikhin L, Urbakh M, Gileadi E (1995) Langmuir 11:674
16. Yang M, Thompson M, Duncan-Hewitt WC (1993) Langmuir 9:802
17. Beck R, Pitterman U, Weil KG (1988) Ber Bunsenges Phys Chem 92:1363
18. Frubose C, Doblhofer K, Soares DM (1993) Ber Bunsenges Phys Chem 97:475
19. Noel MAM, Topart PA (1994) Anal Chem 66:484
20. Bandey HL, Gonsalves M, Hillman AR, Glidle A, Bruckenstein S (1996) J Electroanal Chem 410:219
21. Soares DM, Tenan MA, Wasle S (1998) Electrochim Acta 44:263
22. Yamamoto N, Yamane T, Tatsuma T, Oyama N (1998) Bull Chem Soc Jpn 68:1641
23. Bund A, Schwitzgebel G (1998) Anal Chem 70:2584
24. Wunsche M, Meyer H, Schumacher R (1999) Z Phys Chem 208:225
25. Plausinaitis D, Raudonis R, Daujotis V (2000) Polish J Chem 74:559
26. Bund A, Schwitzgebel G (2000) Electrochim Acta 45:3703
27. Daikhin L, Gileadi E, Katz G, Tsionsky V, Urbakh M, Zagidulin D (2002) Anal Chem 74:554
28. Tsionsky V, Katz G, Gileadi E, Daikhin L (2002) J Electroanal Chem 524:110
29. Martin SJ, Frey GC (1991) IEEE Ultrasonics Symp Proc. IEEE, New York, p 393
30. Johannsmann D, Mathauer K, Wegner G, Knoll W (1992) Phys Rev B 46:7808
31. Glidle A, Hillman AR, Bruckenstein S (1991) J Electroanal Chem 318:411
32. Muramatsu H, Kimura K (1992) Anal Chem 64:2502
33. Yang MS, Chung FL, Thompson M (1993) Anal Chem 65:3713
34. Krim J, Solina DH, Chiarello RP (1991) Phys Rev Let 66:181
35. Krim J, Watts ET, Digel J (1990) J Vac Sci Technol A 8:3417

36. Watts ET, Krim J, Widom A (1990) Phys Rev B 41:3466
37. Krim J, Widom A (1988) Phys Rev B 38:12184
38. Krim J, Chiarello RP (1991) J Vac Sci Technol A 9:2566
39. Persson BNJ (2000) Sliding friction: physical priciples and applications. Springer, Berlin, Heidelberg, New York
40. Daly C, Krim J (1996) Phys Rev Lett 76:803
41. Bruschi L, Carlin A, Mistura G (2002) Phys Rev Lett 88:046105
42. Feynman R (1965) Lectures on physics. In: Reading MA (ed) Lectures on physics. Addison-Wesley, Boston
43. Koplik J, Banavar JR (1995) Annu Rev Fluid Mech 27:257
44. Tsionsky V, Daikhin L, Gileadi E (1996) J Electrochem Soc 143:2240
45. Pit R, Hervet H, Leger L (2000) Phys Rev Lett 85:980
46. Churaev NN, Sobolev VD, Somov AN (1984) J Colloid Int Sci 97:574
47. Krim J (1996) Sci Amer 275:74
48. Cottin-Bizonne C, Barrat JL, Bocquet L, Charlaix E (2003) Nature Mater 2:237
49. Cottin-Bizonne C, Cross B, Steinberger A, Charlaix E (2005) Phys Rev Lett 94:056102
50. Vinogradova OI, Yakubov GE (2003) Langmuir 19:1227
51. Zhu YX, Granick S (2001) Phys Rev Lett 87:096105
52. Craig VSJ, Neto C, Williams DRM (2001) Phys Rev Lett 87:054504
53. Thompson PA, Troian SM (1997) Nature 389:360
54. Gupta SA, Cochran HD, Cummings PT (1997) J Chem Phys 107:10316
55. Neto C, Evans DR, Bonaccurso E, Butt HJ, Craig VSJ (2005) Rep Progr Phys 68:2859
56. Lauga E, Brenner MP, Stone HA, Foss J, Tropea C, Yarin A (eds) (2005) Handbook of experimental fluid dynamics. Springer, Berlin Heidelberg New York
57. Ellis JS, Thompson M (2004) Phys Chem Chem Phys 6:4928
58. de Gennes J-P (1979) C R Acad Sci, Paris B 288:219
59. Barrat JL, Bocquet L (1999) Faraday Discuss 112:119
60. Lumma D, Best A, Gansen A, Feuillebois F, Radler JO, Vinogradova OI (2003) Phys Rev E 67:056313
61. Daikhin L, Gileadi E, Tsionsky V, Urbakh M, Zilberman G (2000) Electrochim Acta 45:3615
62. Becker T, Mugele F (2003) Phys Rev Lett 91:166104
63. Bonaccurso E, Butt HJ, Craig VSJ (2003) Phys Rev Lett 90:144501
64. Zhu YX, Granick S (2002) Phys Rev Lett 88:106102
65. Lin ZQ, Granick S (2003) Langmuir 19:7061
66. Andrienko D, Dunweg B, Vinogradova OI (2003) J Chem Phys 119:13106
67. Rodahl M, Kasemo B (1996) Sensor Actuator A-Phys 54:448
68. Barrat JL, Bocquet L (1999) Phys Rev Lett 82:4671
69. Thompson PA, Robbins MO (1990) Phys Rev A 41:6830
70. Pit R, Hervet H, Leger L (1999) Tribol Lett 7:147
71. Tolstoi DM (1952) Dokl Akad Nauk SSSR 85:1329
72. Blake TD (1990) Colloids Surf 47:135
73. Thompson M, Kipling AL, Duncanhewitt WC, Rajakovic LV, Cavicvlasak BA (1991) Analyst 116:881
74. Kipling AL, Thompson M (1990) Anal Chem 62:1514
75. Bruckenstein S, Fensore A, Li Z, Hillman AR (1994) J Electroanal Chem 370:189
76. Schumacher R, Borges G, Kanazawa KK (1985) Surf Sci 163:L621
77. Schumacher R, Gordon JG, Melory OJ (1987) J Electroanal Chem 216:127
78. Yang M, Thompson M (1993) Langmuir 9:1990

79. Beck R, Pitterman U, Weil KG (1992) J Electroanal Chem 139:453
80. Urbakh M, Daikhin L (1994) Phys Rev B 49:4886
81. Bruschi L, Mistura G (1901) Phys Rev B 6323:5411
82. Urbakh M, Daikhin L (1994) Langmuir 10:2836
83. Daikhin L, Urbakh M (1996) Langmuir 12:6354
84. Sahimi M (1993) Rev Mod Phys 65:1393
85. Jones JL, Marques CM, Joanny JF (1995) Macromolecules 28:136
86. Brinkman HC (1947) Appl Sci Res A 1:27
87. Beck R, Pitterman U, Weil KG (1992) J Electrochem Soc 139:453
88. Bund A, Schneider M (2002) J Electrochem Soc 149:E331
89. Urbakh M, Daikhin L (1994) Phys Rev B 49:4866
90. Wehner S, Wondraczek K, Johannsmann D, Bund A (2004) Langmuir 20:2356
91. Wondraczek K, Bund A, Johannsmann D (2004) Langmuir 20:10346
92. Wilde CP, Zhang MJ (1992) J Electroanal Chem 340:241
93. Raudonis R, Plausinaitis D, Daujotis V (1993) J Electroanal Chem 358:351
94. Tsionsky V, Katz G, Gileadi E, Daikhin L (2002) J Electroanal Chem 524:110
95. Wilde CP, De Cliff SV, Hui KC, Brett DJL (2000) Electrochim Acta 45:3649
96. Uchida H, Ikeda N, Watanabe M (1997) J Electroanal Chem 424:5
97. Mao Y, Hwang E, Scherson D (1995) Anal Chem 67:2415
98. Watanabe M, Uchida H, Ikeda N (1995) J Electroanal Chem 380:255
99. Bruckenstein S, Shay M (1985) J Electroanal Chem 188:131
100. Stockel W, Schumacher R (1987) Ber Bunsenges Phys Chem 91:345
101. Daujotis V, Jasaitis D, Raudonis R (1997) Electrochim Acta 42:1337
102. Jabbarzadeh A, Atkinson JD, Tanner RI (2000) Phys Rev E 61:690
103. Cottin-Bizonne C, Jurine S, Baudry J, Crassous J, Restagno F, Charlaix E (2002) Eur Phys J E 9:47
104. Ponomarev IV, Meyerovich AE (2003) Phys Rev E 67:026302
105. Einzel D, Panzer P, Liu M (1990) Phys Rev Lett 64:2269
106. Panzer P, Liu M, Einzel D (1992) Int J Modern Phys B 6:3251
107. McHale G, Newton MI (2004) J App Phys 95:373
108. Einzel D, Panzer P, Liu M (1990) Phys Rev Lett 64:2269
109. de Gennes PG (2002) Langmuir 18:3413
110. Quere D (2002) Nature Mater 1:14
111. Lauga E, Brenner MP (2004) Phys Rev E 70:026311
112. Du BY, Goubaidoulline E, Johannsmann D (2004) Langmuir 20:10617
113. Ishida N, Sakamoto M, Miyahara M, Higashitani K (2000) Langmuir 16:5681
114. Zhang XH, Jun H (2004) Prog Chem 16:673
115. Tyrrell JWG, Attard P (2001) Phys Rev Lett 87:176104
116. Evans DR, Craig VSJ, Senden TJ (2004) Physica A 339:101
117. Mao M, Zhang JH, Yoon RH, Ducker WA (2004) Langmuir 20:1843
118. Attard P (2003) Adv Colloid Interface Sci 104:75
119. Christenson HK, Claesson PM (2001) Adv Colloid Interface Sci 91:391
120. Tretheway DC, Meinhart CD (2004) Phys Fluids 16:1509
121. Theisen LA, Martin SJ, Hillman AR (2004) Analyt Chem 76:796
122. Tsionsky V, Kaverin A, Daikhin L, Katz G, Gileadi E (2005) Phys Chem Chem Phys 7:1830